Differential Multi-Carrier Faster-Than-Nyquist Signaling in Doubly Selective Fading Channel

Takumi Ishihara, *Member, IEEE*,
and Shinya Sugiura, *Senior Member, IEEE*

***Abstract*—In this article, we propose a novel concept of differentially encoded multi-carrier faster-than-Nyquist (DMFTN) signaling with noncoherent detection, which is robust against a detrimental doubly selective fading channel. In the proposed scheme, by approximately diagonalizing the FTN-specific inter-symbol interference (ISI) and noise correlation matrices, the traditional differential encoding and noncoherent detection algorithm is directly applied to MFTN signaling, which allows us to dispense with any channel state information at the receiver in a dispersive channel. Owing to the reduced frame duration of MFTN signaling, our proposed DMFTN scheme is capable of mitigating detrimental Doppler effects compared to the traditional differentially encoded orthogonal frequency-division multiplexing scheme.**

***Index Terms*—Differential encoding, doubly selective fading channel, faster-than-Nyquist signaling, multi-carrier, noncoherent detection, Nyquist criterion, orthogonal frequency-division multiplexing.**

I. Introduction

Single-carrier faster-than-Nyquist (FTN) signaling [1], [2] has the potential of overcoming the limitation of the classic Nyquist criterion, i.e., the information loss associated with an excess bandwidth. The symbol interval of FTN signaling is set to $T = \tau T_0$ ($0 < \tau \leq 1$), where τ is referred to as a symbol packing ratio, and T_0 is the minimum symbol interval free from inter-symbol interference (ISI). Information-theoretic analyses of FTN signaling can be found in [3], [4], [5], [6], [7]. In [3], Rusek and Anderson revealed that FTN signaling achieves a higher information rate than its conventional Nyquist signaling counterpart when a realistic RRC shaping filter, having an excess bandwidth, is employed. Importantly, the information rate is increased by FTN signaling for $1/(1+\beta) \leq \tau \leq 1$, where β is the roll-off factor of an RRC shaping filter, while no further improvement is achieved for $\tau < 1/(1+\beta)$. Moreover, Kim [4] investigated the capacity of FTN signaling precoded by an orthogonal matrix calculated by the eigenvalue decomposition (EVD) of an FTN-specific ISI matrix. To further improve the information rate, EVD-precoded FTN signaling with optimal power allocation was developed in a number of studies [2], [5], [6], [8], where the optimal power allocation that maximizes the achievable information rate was derived. More specifically, EVD-precoded FTN signaling with optimal power allocation employing a realistic RRC shaping filter ($\beta > 0$) was shown to achieve an information rate identical to the theoretical upper bound (Shannon capacity) of Nyquist signaling, which is achieved by the idealistic rectangular shaping filter ($\beta = 0$). Moreover, in [7], EVD-precoded FTN signaling with optimal power allocation was extended to that supporting a frequency-selective fading channel while allowing a marginal information rate loss. In [9], reduced-complexity fast Fourier transform (FFT)-spread multi-carrier FTN (MFTN) signaling with power allocation was proposed, which achieves a bit-error-ratio (BER) performance close to the bound achieved by its full-complexity counterpart [7] that is information-rate-sense optimal while significantly reducing the computational complexity to $\mathcal{O}(N \log N)$, where N denotes the transmission block size

As mentioned in [7], [10], single-carrier FTN signaling may have the potential of achieving additional gain relative to its Nyquist signaling counterpart in a rapidly time-varying channel because the symbol interval of FTN signaling is smaller than that of Nyquist signaling. However, no extensive performance investigation and analysis of such a gain of FTN signaling in a time-varying channel have been reported. Additionally, the transmitter of EVD-precoded FTN signaling [7], [10] requires feedback from the receiver to acquire accurate channel state information (CSI) in addition to excessively high computational complexity, and hence its direct application to a time-varying channel is not realistic. Furthermore, in [11], differential encoding and noncoherent detection were applied to single-carrier FTN signaling. However, the scenarios applicable by [11] are limited to the frequency-flat channels.

Against the above-mentioned background, the novel contributions of this paper are as follows: Motivated by low-complexity MFTN signaling proposed in [9], we propose a novel concept of open-loop differentially encoded MFTN (DMFTN) signaling and its noncoherent detection, which allows us to dispense with any CSI at either transmitter or receiver. The main merits of the proposed scheme are four-hold. First, since FTN signaling is capable of reducing a symbol interval as far as $\tau \geq 1/(1+\beta)$ without imposing any information rate loss, the effect of Doppler shift, dominated by a symbol interval, is significantly reduced. Second, our noncoherent MFTN detection allows us to dispense with any channel estimation at the receiver, even in a frequency-selective channel, unlike the conventional noncoherent MFTN signaling, which is also robust against the existing coherent counterpart suffering from potential channel estimation errors. Third, the proposed scheme is constituted by an open-loop structure, and hence our transmitter does not need any feedback from the receiver, unlike the conventional MFTN of [9]. Fourth, the FFT-based diagonalization significantly reduces the computational complexity in comparison to the optimal EVD-based counterpart [7], [10] without sacrificing any substantial performance loss.

II. System Model

A. Coherent MFTN Signaling Without Cyclic-Prefix Insertion

In this section, we review the system model of conventional open-loop (unprecoded) coherent MFTN signaling. First, the frequency-domain (FD) information symbols $\mathbf{s}_k = [s_{k,0}, s_{k,1}, \ldots, s_{k,N-1}]^T \in \mathbb{C}^N$, where $s_{k,n}$ represents the $\mathcal{M}$-point phase-shift keying (PSK) symbol on the nth subcarrier in the kth transmit frame, are transformed into their time-domain (TD) counterparts as follows:

$$\mathbf{x}_k = [x_{k,0}, x_{k,1}, \ldots, x_{k,N-1}]^T \in \mathbb{C}^N \tag{1}$$

$$= \mathbf{Q}^H \mathbf{s}_k, \tag{2}$$

where $\mathbf{Q} \in \mathbb{C}^{N \times N}$ denotes the normalized discrete Fourier transform (DFT) matrix, whose mth-row and lth-column entry is defined by

Manuscript received 30 December 2022; revised 25 May 2023; accepted 14 August 2023. Date of publication 16 August 2023; date of current version 17 January 2024. The work of Shinya Sugiura was supported by Japan Science and Technology Agency (JST) FOREST under Grant JPMJFR2127, and in part by JSPS KAKENHI under Grant 22H01481. The review of this article was coordinated by Prof. Xianbin Wang. *(Corresponding author: Shinya Sugiura.)*

The authors are with the Institute of Industrial Science, The University of Tokyo, Tokyo 153-8505, Japan (e-mail: t.ishihara@ieee.org; sugiura@iis.u-tokyo.ac.jp).

Digital Object Identifier 10.1109/TVT.2023.3305731

$(1/\sqrt{N})\exp[-2\pi j(m-1)(l-1)/N]$. We assume $\mathbb{E}[|s_k|^2]=\sigma_s^2=1$, where $\mathbb{E}[\cdot]$ is the expectation operation. Then, the TD symbols $\mathbf{x}_k$ are passed through an RRC shaping filter having the impulse response $q(t)$ with the symbol interval $T=\tau T_0$. When successively transmitting the K MFTN frames, the corresponding transmit signal is represented by

$$x(t)=\sum_{k=0}^{K-1}\sum_{n=0}^{N-1}x_{k,n}q(t-(n+k)T). \tag{3}$$

Note that the MFTN signal with $\tau=1$ and $\beta=0$ corresponds to the conventional OFDM signal.

Assuming an L-tap fading channel, the received signal after passing through a matched filter $q^*(-t)$ at the receiver is given by [12]

$$y(t)=x(t)\otimes h(t,\gamma)\otimes q^*(t)+n(t)\otimes q^*(t) \tag{4}$$

$$=\sum_{k=0}^{K-1}\sum_{n=0}^{N-1}\sum_{l=0}^{L-1}h_l(t)x_{k,n}g(t-(n+k)T-\gamma_l)+\eta(t), \tag{5}$$

where $\otimes$ represents the convolution operation, while we have $g(t)=\int_{-\infty}^{\infty}q(\zeta)q^*(t-\zeta)d\zeta$ and $\eta(t)=\int_{-\infty}^{\infty}n(\zeta)q^*(t-\zeta)d\zeta$. Furthermore, $n(t)$ represents a complex-valued Gaussian random signal, having a power spectral density of N_0. Moreover, $h(t,\gamma)$ represents the impulse response of an L-tap doubly selective fading channel, which is defined as follows: $h(t,\gamma)=\sum_{l=0}^{L-1}h_l(t)\delta(\gamma-\gamma_l)$ [13], where γ_l denotes the propagation delay of the lth path, while $\delta(\cdot)$ is the delta function. Furthermore, $h_l(t)$ represents the lth-tap complex-valued channel coefficient at time t, which has the correlation defined by $\mathbb{E}[h_l(t)h_l^*(t+m)]=J_0(2\pi m F_\mathrm{d})$, where F_d is the normalized Doppler frequency and $J_0(\cdot)$ is the zero-order Bessel function of the first kind. By sampling $y(t)$ at $t=mT$ $(m=0,1,\ldots,KN-1)$, the received sample is obtained as

$$y(mT)=\sum_{k=0}^{K-1}\sum_{n=0}^{N-1}\sum_{l=0}^{L-1}h_l(mT)x_{k,n}g((m-(n+k))T-\gamma_l)+\eta(mT), \tag{6}$$

where the noise samples $\eta(mT)$ $(m=0,1,\ldots,KN-1)$ have an FTN-specific correlation of $\mathbb{E}[\eta(\xi T)\eta^*(\zeta T)]=N_0g((\xi-\zeta)T)$. The correlation between the channel coefficients $h_l(\xi T)$ and $h_l((\xi+\zeta)T)$ is defined by

$$\mathbb{E}\left[h_l(\xi T)h_l^*\left((\xi+\zeta)T\right)\right]=J_0\left(2\pi\zeta\tau F_\mathrm{d}T_0\right). \tag{7}$$

Note that the channel correlation depends on the symbol packing ratio τ [7], as shown in (7).

B. CP-Assisted Coherent MFTN Signaling

We next present the system model of CP-assisted MFTN signaling [9], where we assume a quasi-static frequency-selective fading channel for the sake of explanation. At the transmitter, the 2ν-length CP symbols $[x_{k,0},x_{k,1},\ldots,x_{k,2\nu-1}]^T$ are added to the end of $\mathbf{x}_k$ as follows:

$$\mathbf{a}_k=[a_{k,0},\ldots,a_{k,N+2\nu-1}]^T\in\mathbb{C}^{N+2\nu} \tag{8}$$

$$=[x_{k,0},\ldots,x_{k,N-1},x_{k,0},\ldots,x_{k,2\nu-1}]^T \tag{9}$$

$$=\mathbf{A}_\mathrm{cp}\mathbf{x}_k, \tag{10}$$

where

$$\mathbf{A}_\mathrm{cp}=\begin{bmatrix}\mathbf{0}_{2\nu\times(N-2\nu)} & \mathbf{I}_{2\nu}\\ & \mathbf{I}_N\end{bmatrix}\in\mathbb{R}^{(N+2\nu)\times N}, \tag{11}$$

and $\mathbf{0}_{2\nu\times(N-2\nu)}$ is the $(2\nu\times(N-2\nu))$-sized zero matrix. The received signal is represented by

$$y(t)=\sum_{k=0}^{K-1}\sum_{n=0}^{N-1}\sum_{l=0}^{L-1}h_la_{k,n}g(t-(n+k)T-\gamma_l)+\eta(t). \tag{12}$$

By removing the first and last ν samples in the kth received frame $\mathbf{y}_k=[y(k(N+2\nu)T),\ldots,y((k+1)(N+2\nu-1)T]^T$, the kth N-length received frame is obtained as [9][1]

$$\mathbf{r}_k=[r_{k,0},\ldots,r_{k,N-1}]^T\in\mathbb{C}^N \tag{13}$$

$$=\mathbf{R}_\mathrm{cp}\mathbf{G}_\mathrm{h}\mathbf{A}_\mathrm{cp}\mathbf{x}+\boldsymbol{\eta} \tag{14}$$

where $\mathbf{R}_\mathrm{cp}=[\mathbf{0}_{N\times\nu}\ \mathbf{I}_N\ \mathbf{0}_{N\times\nu}]\in\mathbb{R}^{N\times(N+2\nu)}$. Moreover, $\mathbf{G}_\mathrm{h}$ in (14) is the $((N+2\nu)\times(N+2\nu))$-sized FTN-specific ISI matrix, whose ath-row and bth-column entry is given by $\mathbf{G}_h(a,b)=\sum_{l=0}^{L-1}h_lg((a-b)T-\gamma_l)$. Furthermore, by assuming $g(aT)=0$ for $|a|>\nu$, the received frame (14) is approximated as [14], [15]

$$\mathbf{r}_k\simeq\mathbf{G}_\mathrm{c}\mathbf{x}_k+\boldsymbol{\eta}. \tag{15}$$

The matrix $\mathbf{G}_\mathrm{c}\in\mathbb{C}^{N\times N}$ in (15) is a circulant matrix.

Based on the EVD, $\mathbf{G}_\mathrm{c}$ is factorized into $\mathbf{G}_\mathrm{c}=\mathbf{Q}^H\boldsymbol{\Lambda}\mathbf{Q}$, where $\boldsymbol{\Lambda}=\mathrm{diag}\{\lambda_0,\ldots,\lambda_{N-1}\}\in\mathbb{C}^{N\times N}$ is the diagonal matrix whose diagonal entries are computed by the FFT of the first column of $\mathbf{G}_\mathrm{c}$. Furthermore, $\boldsymbol{\eta}$ is the correlated noise components having the FTN-specific correlation matrix $\mathbb{E}[\boldsymbol{\eta}\boldsymbol{\eta}^H]=N_0\mathbf{G}$, where $\mathbf{G}\in\mathbb{R}^{N\times N}$ is a Toeplitz matrix, whose first column and first row are given by $[g(0),g(T),\ldots,g((N-1)T)]^T$ and $[g(0),g(-T),\ldots,g(-(N-1)T)]$, respectively.

As mentioned in [9], for sufficiently large N and in the range of $\tau>1/(1+\beta)$, $\mathbf{G}$ is approximated by a circulant matrix as follows: $\mathbf{G}\simeq\mathbf{Q}^H\boldsymbol{\Psi}\mathbf{Q}$, where $\boldsymbol{\Psi}=\mathrm{diag}\{\psi_0,\ldots,\psi_{N-1}\}\in\mathbb{R}^{N\times N}$ is a diagonal matrix having the diagonal elements computed by the FFT of $\mathbf{g}=[g(0),g(T),\ldots,g(mT),0,\ldots,0,g(-mT),\ldots,g(-T)]^T$ $(0\le m\le\lceil N/2-1\rceil)$. Similar to [9], we assume $m=\lceil N/2-1\rceil$.

Therefore, by multiplying $\mathbf{Q}$ by (15), the received frame is approximately diagonalized as follows:

$$\mathbf{r}_{k,\mathrm{d}}=\mathbf{Q}\mathbf{r}_k \tag{16}$$

$$=\boldsymbol{\Lambda}\mathbf{s}_k+\boldsymbol{\eta}_\mathrm{f}, \tag{17}$$

where $\boldsymbol{\eta}_\mathrm{f}=[\eta_{\mathrm{f},0},\ldots,\eta_{\mathrm{f},N-1}]^T=\mathbf{Q}\boldsymbol{\eta}$. The noise components $\boldsymbol{\eta}_\mathrm{f}$ are approximately whitened as follows: $\mathbb{E}[\boldsymbol{\eta}_\mathrm{f}\boldsymbol{\eta}_\mathrm{f}^H]=N_0\mathbf{Q}\mathbf{G}\mathbf{Q}^H\simeq N_0\boldsymbol{\Psi}$.

III. Proposed DMFTN Signaling

In this section, we propose a novel open-loop DMFTN signaling, having a high resilience against the effects of Doppler shift owing to the reduced frame interval.

A. Transmitter Structure

At the transmitter, the information symbols are differentially encoded over the successive transmit MFTN frames as follows:

$$d_{k,n}=d_{k-1,n}s_{k,n}\quad\text{for}\quad k\ge1, \tag{18}$$

where $d_{k,n}$ denotes the $\mathcal{M}$-point differentially encoded PSK (DPSK) symbol on the nth subcarrier in the kth transmit frame, and we assume

[1]Note that (14) holds when sufficiently long CP symbols are added and the detrimental effects of inter-frame interference (IFI) are ignored.

$d_{0,n} = 1$ for simplicity.[2] Then, the TD symbols are given by

$$\mathbf{c}_k = \mathbf{Q}^H \mathbf{d}_k, \tag{19}$$

where $\mathbf{d}_k = [d_{k,0}, \ldots, d_{k,N-1}]^T$. Moreover, the 2ν-length CP symbols are added to the kth transmit frame $\mathbf{c}_k$ as follows:

$$\mathbf{e}_k = [e_{k,0}, \ldots, e_{k,N+2\nu-1}]^T \in \mathbb{C}^{N+2\nu} \tag{20}$$

$$= [c_{k,0}, \ldots, c_{k,N-1}, c_{k,0}, \ldots, c_{k,2\nu-1}]^T \tag{21}$$

$$= \mathbf{A}_{\text{cp}} \mathbf{c}_k. \tag{22}$$

In this paper, we consider the successive transmission of the $(K+1)$ DMFTN frames to evaluate the effects of a doubly selective channel in a fair manner.

The average transmit energy per frame of the proposed DMFTN signal is calculated as follows: [2], [7] $E = \mathbb{E}[\mathbf{e}^H \mathbf{G} \mathbf{e}] = \sum_{n=0}^{N-1} \phi_k$, where $\mathbf{\Phi} = \mathbf{Q} \mathbf{A}_{\text{cp}}^T \mathbf{G}_{N+2\nu} \mathbf{A}_{\text{cp}} \mathbf{Q}^H$, and ϕ_k is the kth diagonal entry of $\mathbf{\Phi}$. Moreover, $\mathbf{G}_{N+2\nu} \in \mathbb{R}^{(N+2\nu)\times(N+2\nu)}$ is a Toeplitz matrix, whose first column and first row are given by $[g(0), g(T), \ldots, g((N+2\nu)T)]^T$ and $[g(0), g(-T), \ldots, g(-(N+2\nu)T)]$, respectively. Therefore, to maintain a constant average transmit energy per frame, irrespective of the CP length 2ν, the transmit symbols d_k is scaled by a factor of $\sqrt{N/\sum_{n=0}^{N-1} \phi_k}$.

B. Receiver Structure

When the CP length is sufficiently longer than the effective IFI length, the kth sampled frame after removing the CP symbols is represented by

$$\mathbf{r}_k = [r_{k,0}, \ldots, r_{k,N-1}]^T \tag{23}$$

$$\simeq \mathbf{G}_{\text{c}} \mathbf{c}_k + \boldsymbol{\eta}, \tag{24}$$

where we assume a quasi-static frequency-selective fading channel for ease of explanation. Note that we consider a doubly selective fading channel in our numerical simulations in Section IV. The sampled frame (24) is diagonalized as follows:

$$\mathbf{t}_k = [t_{k,0}, t_{k,1}, \ldots, t_{k,N-1}]^T \tag{25}$$

$$= \mathbf{Q} \mathbf{r}_k \tag{26}$$

$$= \mathbf{\Lambda} \mathbf{d}_k + \boldsymbol{\eta}_{\text{f}}, \tag{27}$$

Thus, the received sample $t_{k,n}$ is represented by [18], [19]

$$t_{k,n} = \lambda_n d_{k,n} + \eta_{\text{f},n} \tag{28}$$

$$= \lambda_n d_{k-1,n} s_{k,n} + \eta_{\text{f},n}. \tag{29}$$

By assuming a static fading channel over the two symbol intervals, we have $t_{k-1,n} = \lambda_n d_{k-1,n} + \eta_{\text{f},n}$. Then, (29) is further modified to

$$t_{k,n} = \lambda_n d_{k-1,n} s_{k,n} + \eta_{\text{f},n} \tag{30}$$

$$= t_{k-1,n} s_{k,n} + \eta_{\text{f},n} - \eta_{\text{f},n} s_{k,n}. \tag{31}$$

Hence, similar to conventional TD DOFDM, the data symbol is estimated in a noncoherent manner without requiring any CSI as follows:

$$\hat{s}_{k,n} = \arg \min_{s_{k,n} \in \mathcal{S}} \left[|t_{k,n} - t_{k-1,n} s_{k,n}|^2 \right], \tag{32}$$

[2]Unlike the TD differential encoding scheme employed in this paper, the differential encoding can also be carried out in the FD, i.e., the data symbols can also be differentially encoded over the successive subcarriers in the same transmit frame [16], [17].

where $\mathcal{S}$ denotes the legitimate set of $s_{k,n}$. The receiver complexity of our DMFTN signaling scheme is dominated by the FFT operation of (26), whose complexity is as low as $\mathcal{O}(N \log N)$ [9].

To elaborate a little further, since precoding is deactivated in the proposed DMFTN signaling scheme, unlike [7], [10], the CSI feedback from the receiver to the transmitter is not needed. This allows us to construct an open-loop transceiver structure, which is free from any feedback delay.

Additionally, note that there have been other schemes [20], [21], such as re-sampling and pilot-based Doppler compensation, which are developed to reduce the effects of the Doppler shift in the doubly selective fading channel. However, our scheme relies on the reduction of a symbol interval by employing FTN signaling, which is different from [20], [21]. Hence, amalgamating the proposed scheme with [20], [21] may further improve the achievable performance while the detailed investigation is beyond the scope of this paper.

C. Three-Stage-Concatenated Turbo-Coded Architecture

At the transmitter, the information bits are encoded by a recursive systematic coding (RSC) encoder. Then, the RSC-encoded bits are interleaved by the outer interleave Π_1. The interleaved bits are further encoded by a unity rate coding (URC) encoder, and the URC-encoded bits are interleaved again by the second interleaver Π_2. The channel-encoded bits are then input into our DMFTN signaling block, including the DPSK, the IFFT, and the CP blocks. Here, we employ the half-rate RSC encoder, which has a constraint length of two and octal generator polynomial $(3, 2)_8$.

At the receiver, after matched-filtering, sampling, CP removal, and FFT-aided diagonalization, the iterative turbo decoding is carried out between the three soft-input soft-output (SISO) decoders, i.e., the log-likelihood ratio (LLR) calculator, the URC decoder, and the RSC decoder. The number of outer decoding iterations between the URC and the RSC decoders and that of inner decoding iterations between the URC and LLR calculation blocks are represented by I_{out} and I_{in}, respectively. After the I_{out} outer iterations, the estimated information bits are output from the RSC decoder.

Based on Bayes' formula, the LLR of the ith bit $b_{i,k,n}$ associated with the received sample $t_{k,n}$ is computed as

$$L(b_{i,k,n}|t_{k,n}) = \ln \frac{p\left(b_{i,k,n} = 0 | t_{k,n}\right)}{p\left(b_{i,k,n} = 1 | t_{k,n}\right)} \tag{33}$$

$$= L_{\text{e}}\left(b_{i,k,n}\right) + L_a\left(b_{i,k,n}\right), \tag{34}$$

where $p(\cdot)$ denotes a probability density function (PDF). Moreover, $L_{\text{e}}(b_{i,k,n})$ and $L_a(b_{i,k,n})$ in (34) represent the extrinsic LLR and the *a priori* LLR, respectively, which are defined by

$$L_{\text{e}}(b_{i,k,n}) = \ln \frac{\sum_{s_{k,n} \in \mathcal{S}_0} p\left(t_{k,n}|s_{k,n}\right) \exp\left(L_i\right)}{\sum_{s_{k,n} \in \mathcal{S}_1} p\left(t_{k,n}|s_{k,n}\right) \exp\left(L_i\right)} \tag{35}$$

$$L_a\left(b_{i,k,n}\right) = \ln \frac{p\left(b_{i,k,n} = 0\right)}{p\left(b_{i,k,n} = 1\right)}, \tag{36}$$

where $L_i = \sum_{m=0, m\neq i}^{B-1} b_{m,k,n} L_a(b_{m,k,n})$. Also, $\mathcal{S}_0$ and $\mathcal{S}_1$ in (35) denote sets of the nth symbol for $b_{i,k,n} = 0$ and for $b_{i,k,n} = 1$, respectively. Moreover, a PDF $p(t_{k,n}|s_{k,n})$ is calculated as

$$p\left(t_{k,n}|s_{k,n}\right) = \frac{1}{\pi 2 \psi_k N_0} \exp\left(-\frac{|t_{k,n} - t_{k-1,n} s_{k,n}|^2}{2 \psi_k N_0} \right). \tag{37}$$

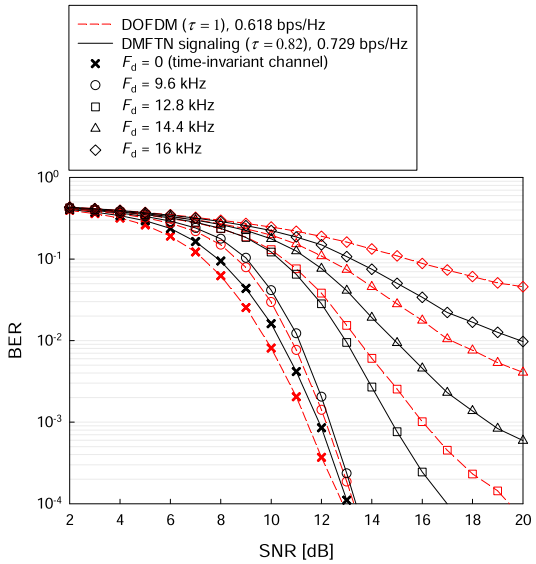

Fig. 1. BER performance of the proposed three-stage turbo-coded DMFTN signaling scheme, where the symbol packing ratio was set to $\tau = 0.82$. The normalized Doppler frequency was set to $F_{\rm d} = 0$, 9.6 kHz, 12.8 kHz, 14.4 kHz, and 16 kHz.

IV. Simulation Results

In this section, we present the simulation results of the achievable BER performance of our proposed three-stage turbo-coded DMFTN signaling system. More specifically, we consider two representative doubly-selective fading channels, i.e., 3GPP TDL-B channel [22], which corresponds to a typical non-line-of-sight (NLOS) 5G communication channel, as well as the underwater acoustic (UWA) communication channel [23].

First, the doubly selective Rayleigh fading of 3GPP TDL-B channel profile [22] was used, where the power of each path was normalized such that the sum of each power becomes unity. The channel coefficients were generated based on the Jakes model to satisfy the correlation of (7), similar to [12], [13], while assuming the 12 scatterers. Moreover, we employed the system parameters of $N = 512$, $K = 10$, $\beta = 0.25$, and $2W(1+\beta) = 100$ MHz, unless otherwise noted.

Fig. 1 shows the achievable BER performance of our proposed DMFTN signaling scheme, where the packing ratio was set to $\tau = 0.82$. For the normalized Doppler frequency, we considered $F_{\rm d} = 9.6$ kHz, 12.8 kHz, 14.4 kHz, and 16 kHz. The CP length was set to $\nu = 50$ and $\nu = 61$ for $\tau = 1$ and $\tau = 0.82$, respectively, while differential quadrature phase-shift keying and the the number of subcarriers of $N = 512$ were employed. Hence, the spectral efficiency was given by 0.618 bps/Hz and 0.729 bps/Hz for $\tau = 1$ and $\tau = 0.82$, respectively. Additionally, we plotted the BER bounds for the time-invariant channel ($F_{\rm d} = 0$). For comparison, we also plotted the curves of the conventional DOFDM scheme ($\tau = 1$). As shown in Fig. 1, for the time-invariant and slowly time-varying scenarios of $F_{\rm d} = 0$ and 9.6 kHz, the BER performance of the proposed DMFTN signaling scheme was slightly lower than its DOFDM counterpart. By contrast, our proposed DMFTN signaling outperformed conventional DOFDM in the higher Doppler frequency scenarios with $F_{\rm d} \geq 12.8$ kHz while benefitting from the rate enhancement effect of MFTN signaling. This is because the frame duration of DMFTN signaling is smaller than its DOFDM counterpart, and hence the detrimental effects of the channel's time-selectivity are mitigated.

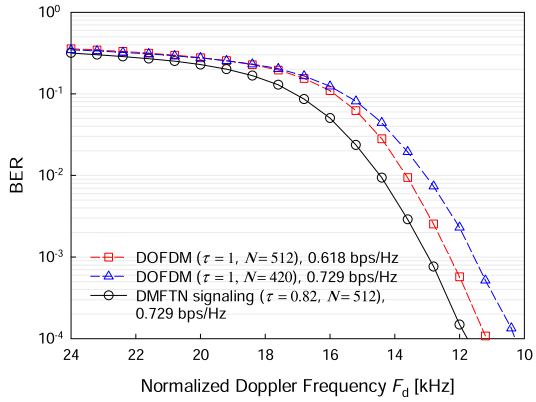

Fig. 2. BER performance of the proposed three-stage turbo-coded DMFTN signaling scheme with $\tau = 0.82$, where the SNR was fixed at 15 dB. The normalized Doppler frequency $F_{\rm d}$ was varied from 24 kHz to 10 kHz in steps of 1 kHz.

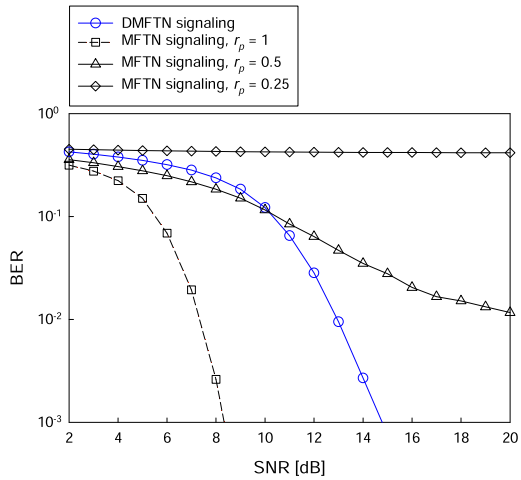

Fig. 3. BER comparisons of the three-stage-concatenated turbo-coded DMFTN and MFTN signaling schemes, where we employed $\tau = 0.82$ and $F_{\rm d} = 12.8$ kHz.

Fig. 2 shows the BER performances of our proposed DMFTN signaling with $\tau = 0.82$ and conventional OFDM ($\tau = 1$), where the normalized Doppler frequency $F_{\rm d}$ was varied from 24 kHz to 10 kHz in steps of 1 kHz. The CP length was set to $\nu = 50$ and 61 for $\tau = 1$ and 0.82, respectively. The target SNR was fixed at 15 dB. Note that in conventional DOFDM, the one possible solution for mitigating detrimental Doppler effects is to shorten the frame length while accepting a sacrifice in the form of an increase in CP loss. Hence, for comparison, we plotted the BER performance of the DOFDM scheme with $N = 420$, whose frame duration is almost identical to that of the DMFTN scheme with $N = 512$ and $\tau = 0.82$, where the spectral efficiency was set to be the same as the DMFTN scheme (0.729 bps/Hz).[3] As shown in Fig. 2, it was found that our proposed DMFTN signaling scheme achieved the best performance in the entire $F_{\rm d}$ range.

Fig. 3 shows the BER comparisons between the proposed DMFTN signaling scheme and the conventional MFTN signaling scheme, where the Doppler frequency was given by $F_d = 12.8$ kHz, and the other

[3]In the conventional DOFDM scheme with $N = 420$, the 0.729 bps/Hz spectral efficiency was achieved by simultaneously using DQPSK and the 8-DPSK.

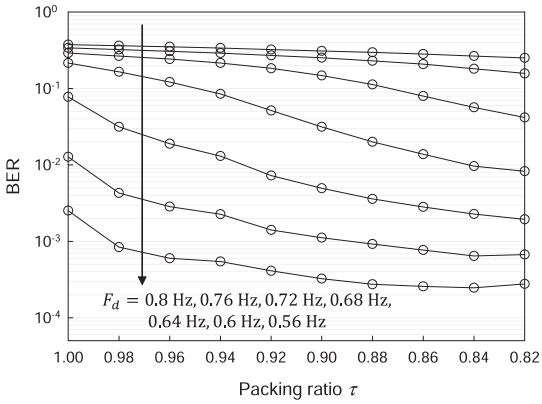

Fig. 4. BER performance of the proposed three-stage turbo-coded DMFTN signaling scheme in the UWA channel at an SNR of 20 dB. The normalized Doppler frequency $F_{\rm d}$ was varied from 0.8 Hz to 0.56 Hz.

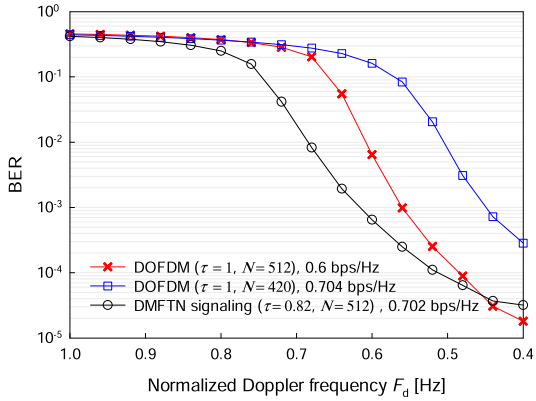

Fig. 5. BER performance of the proposed three-stage turbo-coded DMFTN signaling scheme with $\tau = 0.82$ in a UWA channel at an SNR of 20 dB. The normalized Doppler frequency $F_{\rm d}$ was varied from 1 Hz to 0.4 Hz.

simulation parameters were the same as those used in Fig. 1.[4] We considered a parameter r_p, which represents the insertion ratio of the number of pilot blocks over that of data blocks. For example, $r_p = 1$ indicates that a single pilot block was inserted for each data block, while $r_p = 0.5$ means that a single pilot block is inserted for every two data blocks. Also, we assumed that in the MFTN signaling scheme, the idealistic perfect CSI was acquired at the beginning of the data block, i.e., just after the pilot block. Observe in Fig 3 that the conventional MFTN signaling scheme with $r_p = 0.5$ and that with 0.25 exhibited the worse BER performance than the proposed DMFTN signaling scheme due to the effects of channel estimation errors. By contrast, the conventional MFTN signaling scheme with $r_p = 1$ outperformed the proposed DMFTN signaling scheme, which is because of the idealistic perfect CSI assumption at the beginning of every data block. Additionally, it is confirmed in our extensive simulations that the proposed DMFTN signaling scheme outperforms the conventional MFTN signaling scheme when the mean square error between the estimated and actual CSI is higher than 0.01.

Next, to evaluate the achievable BER performance of the proposed DMFTN scheme in a doubly selective fading channel under more severe conditions, we show the simulation results in a UWA communication channel. We considered the UWA channel profile reported in [23]. In the rest of this section, we considered the bandwidth of $2W(1+\beta) = 5$ kHz. Due to the significantly low propagation speed of sound underwater (1500 m/s), the UWA channel is inherently broadband despite having a low bandwidth of 5 kHz, and the channel suffers from severe Doppler effects even with a small motion of the terminal [23]. Similar to [16], [25], we assumed that the channel coefficients are phase-rotated due to the Doppler effects as follows: $h_l(\xi T) = h_l(0)e^{j2\pi\xi\tau F_{\rm d}T_0}$.

Fig. 4 shows the achievable BER performance in the UWA communication channel, where the packing ratio was varied from $\tau = 1$ to 0.82 in steps of 0.02. The CP length was set to $\nu = 60$, 61, 62, 63, 64, 66, 68, 70, 72, and 74 for $\tau = 1$, 0.98, 0.96, 0.94, 0.92, 0.9, 0.88, 0.86, 0.84, and 0.82, respectively. The normalized Doppler frequency $F_{\rm d}$ was set to 0.8 Hz, 0.76 Hz, 0.72 Hz, 0.68 Hz, 0.64 Hz, 0.6 Hz, and 0.56 Hz, which correspond to the velocities 0.346 km/h, 0.328 km/h, 0.311 km/h, 0.294 km/h, 0.277 km/h, 0.259 km/h, and 0.242 km/h, respectively, for a carrier frequency of 12.5 kHz. Finally, the SNR was fixed at 20 dB. In Fig. 4, it was found that for $F_{\rm d} \geq 0.64$ Hz, the BER of the proposed DMFTN scheme decreased upon decreasing the packing ratio τ while outperforming its conventional DOFDM counterpart ($\tau = 1$).

Moreover, Fig. 5 shows the BER performance of the proposed DMFTN scheme with $\tau = 0.82$, where the Doppler frequency $F_{\rm d}$ was varied from 1 Hz to 0.4 Hz in steps of 0.04 Hz. The SNR was fixed at 20 dB. Similar to Fig. 2, we plotted the BER performance of the DOFDM scheme ($\tau = 1$, $N = 512$) with the same frame duration and spectral efficiency as the DMFTN scheme for comparison. As shown in Fig. 5, while the conventional DOFDM scheme having $N = 512$ exhibited a marginal performance advantage in the slowly time-varying scenarios of $F_{\rm d} = 0.44$ Hz and 0.4 Hz,[5] our proposed DMFTN signaling scheme outperformed the DOFDM benchmark schemes over the entire regime of $F_{\rm d} \geq 0.48$ Hz.

V. Conclusion

In this paper, we proposed the novel concept of low-complexity DMFTN signaling, which allows us to dispense with any CSI at either transmitter or receiver in a time-varying dispersive channel. Since the received DMFTN signals are approximately diagonalized by relying on the circulant-matrix approximation of the FTN-specific ISI and noise correlation matrices, noncoherent detection is enabled. As the explicit benefits of the reduced frame duration of our MFTN signaling, our proposed DMFTN scheme is capable of mitigating detrimental Doppler effects and improving the detection performance in a rapidly time-varying fading scenario.

References

[1] J. E. Mazo, "Faster-than-Nyquist signaling," *Bell Syst. Tech. J.*, vol. 54, no. 8, pp. 1451–1462, Oct. 1975.
[2] T. Ishihara, S. Sugiura, and L. Hanzo, "The evolution of faster-than-Nyquist signaling," *IEEE Access*, vol. 9, pp. 86535–86564, 2021.
[3] F. Rusek and J. B. Anderson, "Constrained capacities for faster-than-Nyquist signaling," *IEEE Trans. Inf. Theory*, vol. 55, no. 2, pp. 764–775, Feb. 2009.

[4] Also, as shown in [24], the additional 4ν-length pilot block is required for channel estimation in the MFTN signaling scheme. Hence, in the MFTN signaling scheme, the number of transmission bits per symbol was varied such that the spectral efficiency became the same as that of the proposed DMFTN signaling scheme.

[5] This slight performance disadvantage of the proposed scheme is induced because the proposed scheme is designed especially for mitigating the effects of a high Doppler frequency. Hence, in the scenario of a low Doppler frequency or in the time-invariant channel, the benefits of our scheme cannot be exploited.

[4] Y. J. D. Kim, "Properties of faster-than-Nyquist channel matrices and folded-spectrum, and their applications," in *Proc. IEEE Wireless Commun. Netw. Conf.*, Doha, Qatar, 2016, pp. 1–7.
[5] T. Ishihara and S. Sugiura, "SVD-precoded faster-than-Nyquist signaling with optimal and truncated power allocation," *IEEE Trans. Wireless Commun.*, vol. 18, no. 12, pp. 5909–5923, Dec. 2019.
[6] T. Ishihara and S. Sugiura, "Comments on and corrections to "SVD-precoded faster-than-Nyquist signaling with optimal and truncated power allocation," 2021, *TechRxiv*, doi: 10.36227/techrxiv.14949681.v1.
[7] T. Ishihara and S. Sugiura, "Eigendecomposition-precoded faster-than-Nyquist signaling with optimal power allocation in frequency-selective fading channel," *IEEE Trans. Wireless Commun.*, vol. 21, no. 3, pp. 1681–1693, Mar. 2022.
[8] S. Sugiura, "Secrecy performance of eigendecomposition-based FTN signaling and NOFDM in quasi-static fading channels," *IEEE Trans. Wireless Commun.*, vol. 20, no. 9, pp. 5872–5882, Sep. 2021.
[9] T. Ishihara and S. Sugiura, "Reduced-complexity FFT-spread multicarrier faster-than-Nyquist signaling in frequency-selective fading channel," *IEEE Open J. Commun. Soc.*, vol. 3, pp. 530–542, 2022.
[10] J. Zhou, T. Ishihara, and S. Sugiura, "Precoded faster-than-Nyquist signaling for doubly selective underwater acoustic communication channel," *IEEE Wireless Commun. Lett.*, vol. 11, no. 10, pp. 2041–2045, Oct. 2022.
[11] T. Ishihara and S. Sugiura, "Differential faster-than-Nyquist signaling," *IEEE Access*, vol. 6, pp. 4199–4206, 2018.
[12] Q. Shi, N. Wu, X. Ma, and H. Wang, "Frequency-domain joint channel estimation and decoding for faster-than-Nyquist signaling," *IEEE Trans. Commun.*, vol. 66, no. 2, pp. 781–795, Feb. 2018.
[13] A. Goldsmith, *Wireless Communications*. Cambridge, U.K.: Cambridge Univ. Press, 2005.
[14] S. Sugiura, "Frequency-domain equalization of faster-than-Nyquist signaling," *IEEE Wireless Commun. Lett.*, vol. 2, no. 5, pp. 555–558, Oct. 2013.
[15] S. Sugiura and L. Hanzo, "Frequency-domain-equalization-aided iterative detection of faster-than-Nyquist signaling," *IEEE Trans. Veh. Technol.*, vol. 64, no. 5, pp. 2122–2128, May 2015.
[16] J. Han, L. Zhang, Q. Zhang, and G. Leus, "Eigendecomposition-based partial FFT demodulation for differential OFDM in underwater acoustic communications," *IEEE Trans. Veh. Technol.*, vol. 67, no. 7, pp. 6706–6710, Jul. 2018.
[17] K. Chen-Hu, Y. Liu, and A. G. Armada, "Non-coherent massive MIMO-OFDM down-link based on differential modulation," *IEEE Trans. Veh. Technol.*, vol. 69, no. 10, pp. 11281–11294, Oct. 2020.
[18] C. Xu et al., "Sixty years of coherent versusnon-coherent tradeoffs and the road from 5G to wireless futures," *IEEE Access*, vol. 7, pp. 178246–178299, 2019.
[19] J. Li, M. Wen, X. Cheng, Y. Yan, S. Song, and M. H. Lee, "Differential spatial modulation with gray coded antenna activation order," *IEEE Commun. Lett.*, vol. 20, no. 6, pp. 1100–1103, Jun. 2016.
[20] K. Tu, T. M. Duman, M. Stojanovic, and J. G. Proakis, "Multiple-resampling receiver design for OFDM over doppler-distorted underwater acoustic channels," *IEEE J. Ocean. Eng.*, vol. 38, no. 2, pp. 333–346, Apr. 2013.
[21] B. Li, S. Zhou, M. Stojanovic, L. Freitag, and P. Willett, "Non-uniform Doppler compensation for zero-padded OFDM over fast-varying underwater acoustic channels," in *Proc. OCEANS*, Aberdeen, U.K., 2007, pp. 1–6.
[22] 3GPP, "Study on channel model for frequencies from 0.5 to 100 GHz," Tech. Rep. TR38.901 v14.2.0, Sep. 2017.
[23] M. Stojanovic and J. Preisig, "Underwater acoustic communication channels: Propagation models and statistical characterization," *IEEE Commun. Mag.*, vol. 47, no. 1, pp. 84–89, Jan. 2009.
[24] T. Ishihara and S. Sugiura, "Iterative frequency-domain joint channel estimation and data detection of faster-than-Nyquist signaling," *IEEE Trans. Wireless Commun.*, vol. 16, no. 9, pp. 6221–6231, Sep. 2017.
[25] W. Shi, C. He, Q. Dang, and L. Jing, "Single-carrier with index modulation for underwater acoustic communications," *Appl. Acoust.*, vol. 172, Jan. 2021, Art. no. 107572.